J|A|C|S
ARTICLES
Published on Web 06/21/2006

Spectroscopic and Computational Studies of Co^{1+}Cobalamin: Spectral and Electronic Properties of the "Superreduced" B_{12} Cofactor

Mathew D. Liptak and Thomas C. Brunold*

Contribution from the University of Wisconsin-Madison, Department of Chemistry, 1101 University Avenue, Madison, Wisconsin 53706

Received March 8, 2006; E-mail: brunold@chem.wisc.edu.

Abstract: The 4-coordinate, low-spin cob(I)alamin (Co^{1+}Cbl) species, which can be obtained by heterolytic cleavage of the Co−C bond in methylcobalamin or the two-electron reduction of vitamin B_{12}, is one of the most powerful nucleophiles known to date. The supernucleophilicity of Co^{1+}Cbl has been harnessed by a number of cobalamin-dependent enzymes, such as the B_{12}-dependent methionine synthase, and by enzymes involved in the biosynthesis of B_{12}, including the human adenosyltransferase. The nontoxic nature of the Co^{1+}Cbl supernucleophile also makes it an attractive target for the in situ bioremediation of halogenated waste. To gain insight into the geometric, electronic, and vibrational properties of this highly reactive species, electronic absorption, circular dichroism (CD), magnetic CD, and resonance Raman (rR) spectroscopies have been employed in conjunction with density functional theory (DFT), time-dependent DFT, and combined quantum mechanics/molecular mechanics computations. Collectively, our results indicate that the supernucleophilicity of Co^{1+}Cbl can be attributed to the large destabilization of the Co $3d_{z^2}$-based HOMO and its favorable orientation with respect to the corrin macrocycle, which minimizes steric repulsion during nucleophilic attack. An intense feature in the CD spectrum and a prominent peak in the rR spectra of Co^{1+}Cbl have been identified that may serve as excellent probes of the nucleophilic character, and thus the reactivity, of Co^{1+}Cbl in altered environments, including enzyme active sites. The implications of our results with respect to the enzymatic formation and reactivity of Co^{1+}Cbl are discussed, and spectroscopic trends along the series from Co^{3+}Cbls to Co^{2+}Cbl and Co^{1+}Cbl are explored.

I. Introduction

The cob(I)alamin (Co^{1+}Cbl) "superreduced" B_{12} cofactor state is accessed in enzymatic systems by heterolytic cleavage of the Co−C bond of the methylcobalamin cofactor (MeCbl, Figure 1), which contains a low-spin Co ion in the +3 oxidation state that is equatorially ligated by the four nitrogens of a tetrapyrrole macrocycle, known as the corrin ring, and axially coordinated by a methyl group in the "upper" position and 5,6-dimethylbenzimidazole (DMB) in the "lower" position. The DMB base is the terminus of an intramolecular nucleotide loop bound to the corrin ring at C_{17}.[1−4] At low pH, DMB dissociates from the Co to yield a "base-off" species[5] with spectroscopic properties similar to those of methylcobinamide (MeCbi) in which the nucleotide loop is clipped off at the phosphodiester bond. Reduction of MeCbl to cob(II)alamin (Co^{2+}Cbl) results in the dissociation of the upper axial methyl group.[6−8] Further reduction of Co^{2+}Cbl to Co^{1+}Cbl leads to the loss of the lower axial DMB ligand, providing an alternate pathway to the 4-coordinate, low-spin Co^{1+}Cbl species[5,8,9] that is one of the most powerful nucleophiles known to date.[10,11]

This "supernucleophilicity" of Co^{1+}Cbl has been harnessed by several enzymatic systems, such as the cobalamin-dependent methionine synthase (MetH) as well as adenosyltransferases (ATRs) that catalyze the Co−C bond formation step in the biosynthesis of adenosylcobalamin (AdoCbl).[12−16] In MetH, Co^{1+}Cbl serves to transfer a methyl group from methyltetrahydrofolate to homocysteine, yielding tetrahydrofolate and methionine, which is essential as an amino acid as well as a precursor for adenosylmethionine (AdoMet).[12] In acetogenic bacteria, a

(1) Randaccio, L.; Furlan, M.; Geremia, S.; Slouf, M.; Srnova, I.; Toffoli, D. *Inorg. Chem.* **2000**, *39*, 3403−3413.
(2) Brown, K. L.; Zou, X.; Marques, H. M. *THEOCHEM* **1998**, *453*, 209−224.
(3) Tollinger, M.; Konrat, R.; Krautler, B. *Helv. Chim. Acta* **1999**, *82*, 1596−1609.
(4) Sagi, I.; Chance, M. R. *J. Am. Chem. Soc.* **1992**, *114*, 8061−8066.
(5) Lexa, D.; Saveant, J. M. *Acc. Chem. Res.* **1983**, *16*, 235−243.
(6) Krautler, B.; Keller, W.; Kratky, C. *J. Am. Chem. Soc.* **1989**, *111*, 8938−8940.
(7) Sagi, I.; Wirt, M. D.; Chen, E. F.; Frisbie, S.; Chance, M. R. *J. Am. Chem. Soc.* **1990**, *112*, 8639−8644.
(8) Giorgetti, M.; Ascone, I.; Berrettoni, M.; Conti, P.; Zamponi, S.; Marassi, R. *J. Biol. Inorg. Chem.* **2000**, *5*, 156−166.
(9) Wirt, M. D.; Sagi, I.; Chance, M. R. *Biophys. J.* **1992**, *63*, 412−417.
(10) Schrauzer, G. N.; Deutsch, E.; Windgassen, R. J. *J. Am. Chem. Soc.* **1968**, *90*, 2441−2442.
(11) Schrauzer, G. N.; Deutsch, E. *J. Am. Chem. Soc.* **1969**, *91*, 3341−3350.
(12) Banerjee, R. V.; Frasca, V.; Ballou, D. P.; Matthews, R. G. *Biochemistry* **1990**, *29*, 11101−11109.
(13) Leal, N. A.; Olteanu, H.; Banerjee, R.; Bobik, T. A. *J. Biol. Chem.* **2004**, *279*, 47536−47542.
(14) Bauer, C. B.; Fonseca, M. V.; Holden, H. M.; Thoden, J. B.; Thompson, T. B.; Escalante-Semerena, J. C.; Rayment, I. *Biochemistry* **2001**, *40*, 361−374.
(15) Johnson, C. L. V.; Buszko, M. L.; Bobik, T. A. *J. Bacteriol.* **2004**, *186*, 7881−7887.
(16) Buan, N. R.; Suh, S. J.; Escalante-Semerena, J. C. *J. Bacteriol.* **2004**, *186*, 5708−5714.

10.1021/ja061433q CCC: $33.50

similar methyl-transfer reaction is catalyzed by the corrinoid iron−sulfur protein,[17] and a number of other methyltransferases have been isolated in acetogens and methanogens as well.[18,19] In the human ATR, Co^{2+}Cbl is converted to AdoCbl in a process involving the transient formation of a Co^{1+}Cbl species that is sufficiently nucleophilic to attack the C5′ carbon of the cosubstrate adenosine triphosphate (ATP).[13,20] Finally, a third type of Co^{1+}Cbl-dependent reactions are catalyzed by the reductive dehalogenases, which reductively cleave the carbon−halogen bonds of a wide range of halogenated organic substrates. From a biochemical viewpoint, a particularly intriguing aspect of this reaction is that the energy released can be coupled to ATP biosynthesis in a process known as dehalorespiration. Alternatively, from an environmental viewpoint, these enzymes provide interesting targets because biodegradation constitutes an environmentally friendly option for the decontamination of sites polluted by halogenated hydrocarbons.[21]

In analogy to the enzymatic systems, the free Co^{1+}Cbl cofactor has been demonstrated to dehalogenate polyhalogenated methanes,[22−28] alkanes,[29−32] ethylenes,[24,28,33−41] acetylenes,[36,42] cyclic alkanes,[43,44] aromatic compounds,[24,45] and carboxylic acids[46] in solution. For this reason, Co^{1+}Cbl obtained by the reduction of vitamin B_{12} with titanium(III) citrate, a process

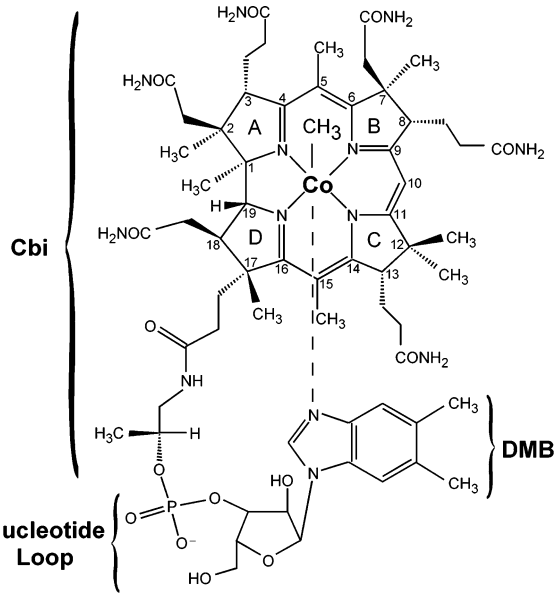

Figure 1. Chemical structure and numbering scheme for methylcobalamin (MeCbl). Note that in Co^{2+}Cbl, the upper axial position is unoccupied, whereas in Co^{1+}Cbl, both axial positions are vacant. In the cobinamide (Cbi) derivatives, the nucleotide loop is clipped off at the phosphodiester bond.

requiring no toxic chemicals, has been targeted as an in situ catalyst for the reductive dechlorination of chlorinated solvents found in contaminated groundwater.[28,47−49] The first step in the reductive dehalogenation of both polyhalogenated methanes and alkanes has been shown by electronic absorption (Abs) spectroscopy to involve a nucleophilic attack of the substrate by Co^{1+}Cbl, forming an alkylcobalamin intermediate.[26,31] The mechanistic details of the reductive dechlorination of polychlorinated ethylenes, however, are still under investigation. A single electron transfer from Co^{1+}Cbl was invoked as the first step in the dechlorination of perchloroethylene (PCE) and trichloroethylene (TCE),[34,50] whereas nucleophilic addition of Co^{1+}Cbl was implicated for the dechlorination of dichloroethylene on the basis of Abs spectroscopic experiments.[35] Yet, recent electrospray mass spectrometry and X-ray crystallographic studies have led to the proposal that the dechlorination of all chlorinated ethylenes by Co^{1+}Cbl actually involves the formation of a chlorovinylcobalamin intermediate.[38,51]

Despite the obvious importance of Co^{1+}Cbl for the function of a wide range of enzymes and the environmentally friendly degradation of chlorinated solvents, relatively little is known about the geometric and electronic properties of this highly reactive species. The Abs spectrum of free Co^{1+}Cbl is characterized by an intense feature near 390 nm and four weaker bands in the visible spectral region (Figure 2).[52] Resonance Raman (rR) spectra of Co^{1+}Cbl obtained previously using 514.5 and 457.9 nm excitation are dominated by vibrational features at 1506, 1534, 1570, and 1596 cm^{-1}, all of which have been

(17) Ragsdale, S. W.; Lindahl, P. A.; Munck, E. *J. Biol. Chem.* **1987**, *262*, 14289−14297.
(18) Ragsdale, S. W. In *Chemistry and Biochemistry of B_{12}*; Banerjee, R., Ed.; John Wiley & Sons: New York, 1999; pp 633−653.
(19) Sauer, K.; Thauer, R. K. In *Chemistry and Biochemistry of B_{12}*; Banerjee, R., Ed.; John Wiley & Sons: New York, 1999; pp 655−679.
(20) Stich, T. A.; Yamanishi, M.; Banerjee, R.; Brunold, T. C. *J. Am. Chem. Soc.* **2005**, *127*, 7660−7661.
(21) Holliger, C.; Wohlfarth, G.; Diekert, G. *FEMS Microbiol. Rev.* **1999**, *22*, 383−398.
(22) Wood, J. M.; Kennedy, F. S.; Wolfe, R. S. *Biochemistry* **1968**, *7*, 1707−1713.
(23) Krone, U. E.; Thauer, R. K.; Hogenkamp, H. P. C. *Biochemistry* **1989**, *28*, 4908−4914.
(24) Gantzer, C. J.; Wackett, L. P. *Environ. Sci. Technol.* **1991**, *25*, 715−722.
(25) Krone, U. E.; Thauer, R. K.; Hogenkamp, H. P. C.; Steinbach, K. *Biochemistry* **1991**, *30*, 2713−2719.
(26) Chiu, P. C.; Reinhard, M. *Environ. Sci. Technol.* **1995**, *29*, 595−603.
(27) Lewis, T. A.; Morra, M. J.; Brown, P. D. *Environ. Sci. Technol.* **1996**, *30*, 292−300.
(28) Lesage, S.; Brown, S.; Millar, K.; Steer, H. *Groundwater Monit. Rem.* **2003**, *23*, 102−110.
(29) Connors, T. F.; Arena, J. V.; Rusling, J. F. *J. Phys. Chem.* **1988**, *92*, 2810−2816.
(30) Schanke, C. A.; Wackett, L. P. *Environ. Sci. Technol.* **1992**, *26*, 830−833.
(31) Holliger, C.; Schraa, G.; Stupperich, E.; Stams, A. J. M.; Zehnder, A. J. B. *J. Bacteriol.* **1992**, *174*, 4427−4434.
(32) Arguello, J. E.; Costentin, C.; Griveau, S.; Saveant, J. M. *J. Am. Chem. Soc.* **2005**, *127*, 5049−5055.
(33) Burris, D. R.; Delcomyn, C. A.; Smith, M. H.; Roberts, A. L. *Environ. Sci. Technol.* **1996**, *30*, 3047−3052.
(34) Glod, G.; Angst, W.; Holliger, C.; Schwarzenbach, R. P. *Environ. Sci. Technol.* **1997**, *31*, 253−260.
(35) Glod, G.; Brodmann, U.; Angst, W.; Holliger, C.; Schwarzenbach, R. P. *Environ. Sci. Technol.* **1997**, *31*, 3154−3160.
(36) Semadeni, M.; Chiu, P. C.; Reinhard, M. *Environ. Sci. Technol.* **1998**, *32*, 1207−1213.
(37) Burris, D. R.; Delcomyn, C. A.; Deng, B. L.; Buck, L. E.; Hatfield, K. *Environ. Toxicol. Chem.* **1998**, *17*, 1681−1688.
(38) Lesage, S.; Brown, S.; Millar, K. *Environ. Sci. Technol.* **1998**, *32*, 2264−2272.
(39) Kim, Y. H.; Carraway, E. R. *Environ. Technol.* **2002**, *23*, 1135−1145.
(40) Slater, G. F.; Lollar, B. S.; Lesage, S.; Brown, S. *Groundwater Monit. Rem.* **2003**, *23*, 59−67.
(41) McCauley, K. M.; Pratt, D. A.; Wilson, S. R.; Shey, J.; Burkey, T. J.; van der Donk, W. A. *J. Am. Chem. Soc.* **2005**, *127*, 1126−1136.
(42) McCauley, K. M.; Wilson, S. R.; van der Donk, W. A. *Inorg. Chem.* **2002**, *41*, 5844−5848.
(43) Ruppe, S.; Neumann, A.; Diekert, G.; Vetter, W. *Environ. Sci. Technol.* **2004**, *38*, 3063−3067.
(44) Rodriguez-Garrido, B.; Arbestain, M. C.; Monterroso, M. C.; Macias, F. *Environ. Sci. Technol.* **2004**, *38*, 5046−5052.
(45) Smith, M. H.; Woods, S. L. *Appl. Environ. Microbiol.* **1994**, *60*, 4111−4115.
(46) Rusling, J. F.; Miaw, C. L.; Couture, E. C. *Inorg. Chem.* **1990**, *29*, 2025−2027.
(47) Zehnder, A. J. B.; Wuhrmann, K. *Science* **1976**, *194*, 1165−1166.
(48) Lesage, S.; Brown, S.; Millar, K. *Groundwater Monit. Rem.* **1996**, *16*, 76−85.
(49) Sorel, D.; Lesage, S.; Brown, S.; Millar, K. *Groundwater Monit. Rem.* **2001**, *21*, 140−148.
(50) Shey, J.; van der Donk, W. A. *J. Am. Chem. Soc.* **2000**, *122*, 12403−12404.
(51) McCauley, K. M.; Wilson, S. R.; van der Donk, W. A. *J. Am. Chem. Soc.* **2003**, *125*, 4410−4411.
(52) Pratt, J. M. *Inorganic Chemistry of Vitamin B_{12}*; Academic Press Inc.: New York, 1972.

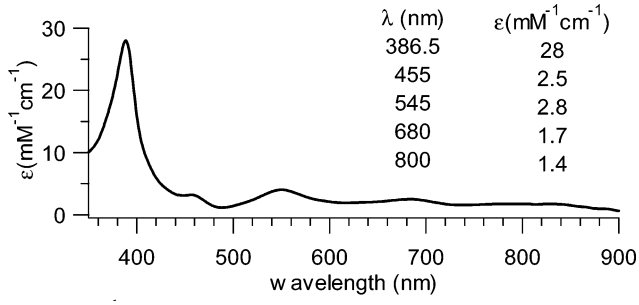

Figure 2. Abs spectrum of Co^{1+}Cbl in a fluid 60:40 mixture of glycerol and NH_4Cl(aq) at 250 K. The peak positions and molar extinction coefficients have been reported previously.[52]

attributed to corrin-based modes.[53,54] Co^{1+}Cbl has also been characterized by X-ray absorption (XAS), and analyses of the extended X-ray absorption fine structure (EXAFS) yielded estimates for the average Co−N bond length of 1.86−1.88 Å.[8,9] Moreover, the electronic structure of Co^{1+}Cbl has been examined using density functional theory (DFT),[55−57] time-dependent DFT (TDDFT),[58] Car-Parinello molecular dynamics,[59] and complete active space multiconfigurational perturbation theory (CASPT2);[60] however, all of these studies have suffered from the fact that insufficient experimental data for Co^{1+}Cbl were available for the validation of computational results.

In this work, we present and discuss Abs and, for the first time, circular dichroism (CD) and magnetic CD (MCD) spectra of Co^{1+}Cbl. We also report the first rR excitation profile data for Co^{1+}Cbl, which are used in conjunction with TDDFT computations to assign key electronic transitions contributing to the Abs, CD, and MCD spectra of Co^{1+}Cbl. The dominant features in the rR spectrum of Co^{1+}Cbl are analyzed within the framework of DFT-based vibrational frequency calculations. On the bases of this analysis and vibrational data for aquacobalamin (H_2OCbl^+),[61] MeCbl,[61] and Co^{2+}Cbl[62] reported in the literature, a correlation is established between the frequency of the corrin ring symmetric short-axis stretch and the partial positive charge localized on the Co center. Additionally, the origin of the "supernucleophilicity" of Co^{1+}Cbl is examined within the context of our computed electronic structure description, and spectroscopic trends along the series from Co^{3+}Cbls[61] to Co^{2+}Cbl[62] and Co^{1+}Cbl are explored.

II. Materials and Methods

Chemicals/Cofactors. H_2OCbl^+, zinc dust, ammonium chloride (NH_4Cl), deuterium chloride (DCl), deuterated water (D_2O), sodium hydroxide (NaOH), and potassium sulfate (K_2SO_4) were purchased from Sigma-Aldrich and used without further purification. All solutions employed in this work were degassed on a vacuum line and sparged with Ar gas. In each case, the solvent used was water unless noted otherwise. Co^{1+}Cbl was obtained by chemical reduction of H_2OCbl^+ with Zn dust under an atmosphere of N_2, using NH_4Cl as the electrolyte, similar to a previously reported procedure.[63] H_2OCbl^+(*d-10*) was used in the place of H_2OCbl^+ to generate Co^{1+}Cbl(*d-10*), whereas H_2OCbl^+-(*d-10*) was prepared by acidification of H_2OCbl^+ with 12 M DCl in D_2O overnight to achieve H/D exchange at the C_{10} position of the corrin ring (Figure 1).[64] Prior to chemical reduction to Co^{1+}Cbl, the pH of H_2OCbl^+(*d-10*) was neutralized with 12 M NaOH in D_2O so as to drastically reduce the rate of H/D exchange at the C_{10} position of the corrin ring.

Spectroscopy. Abs, CD, and MCD spectra of Co^{1+}Cbl were obtained in a 60:40 mixture (v/v) of glycerol and saturated NH_4Cl solution at 250 K under an atmosphere of He. A concentrated sample (0.72 mM in Co^{1+}Cbl) was utilized to collect the data below 22 548 cm^{-1}, while a more dilute sample (0.24 mM) was used above 22 548 cm^{-1}. Concentrations were determined on the basis of published molar extinction coefficients.[52] All spectra presented in this study were obtained with a Jasco J-715 spectropolarimeter in conjunction with an Oxford Instruments SM-4000 8T magnetocryostat. CD contributions to the MCD spectra were eliminated by subtracting the −7 T spectrum from the +7 T spectrum and dividing the resulting trace by 2.

rR spectra of Co^{1+}Cbl and Co^{1+}Cbl(*d-10*) were obtained at 77 K in a frozen 50:50 mixture (v/v) of distilled, deionized water and saturated NH_4Cl. All available laser lines between 568.2 and 363.8 nm of Coherent I-305 Ar^+ and Coherent I-302C Kr^+ lasers were used in these experiments. The scattered light was collected using a ∼135° backscattering arrangement, dispersed by an Acton Research triple monochromator equipped with 1200 and 2400 groves/mm gratings, and analyzed with a Princeton Instruments Spec X: 100BR deep depletion, back-thinned CCD camera. Each rR excitation profile data point presented in this paper represents the average peak intensity observed in at least three separately acquired spectra. Peak positions and intensities for Co^{1+}Cbl were calibrated using either the ice peak at 228 cm^{-1} or the SO_4^{2-} peak at 984 cm^{-1} from the internal standard K_2SO_4.

For the Co^{1+}Cbl(*d-10*) sample, one rR profile was obtained using all available Ar^+ laser lines between 514.1 and 454.5 nm, whereas the peak positions and intensities were calibrated using the ice peak of the frozen 50:50 (v/v) H_2O/D_2O mixture at 225.5 cm^{-1} (average of H_2O and D_2O ice peak positions). The enhancement behavior of all vibrational features was found to be the same in the rR spectra of the deuterated and nondeuterated samples of Co^{1+}Cbl. The isotopic shifts determined by this method were verified for 514.5 and 454.5 nm excitation by the consecutive collection of Co^{1+}Cbl and Co^{1+}Cbl(*d-10*) scattering data without changing the sample dewar position and monochromator settings between samples.

Computations: Geometries and Frequencies. All geometry optimizations and frequency calculations were carried out on a cluster consisting of 64 Intel Xeon processors (ACE Computers) using the Amsterdam Density Functional 2004.01 suite of programs with an integration parameter of 4.0, "conserve points" gradient smoothing, and the TZP basis set (formerly called basis set IV) with a frozen core through 1s (C, N, O) or 2p (Co).[65−67] The geometry optimizations used the following convergence criteria: 0.0001 Hartree in the total energy, 0.001 Hartree/Å in the Cartesian gradients, and 0.001 Å in the estimated uncertainty of the Cartesian coordinates. To calculate harmonic frequencies, the two-point numerical differentiation approach with ±0.01 Å Cartesian coordinate displacements of the atoms was employed.[68,69] The off-resonance Raman scattering intensities and

(53) Mayer, E.; Gardiner, D. J.; Hester, R. E. *Mol. Phys.* **1973**, *26*, 783−787.
(54) Mayer, E.; Gardiner, D. J.; Harder, S. R. *J. Chem. Soc., Faraday Trans. 2* **1973**, *69*, 1350−1358.
(55) Dolker, N.; Maseras, F.; Lledos, A. *J. Phys. Chem. B* **2003**, *107*, 306−315.
(56) Jensen, K. P.; Ryde, U. *ChemBioChem* **2003**, *4*, 413−424.
(57) Pratt, D. A.; van der Donk, W. A. *J. Am. Chem. Soc.* **2005**, *127*, 384−396.
(58) Jaworska, M.; Lodowski, P. *THEOCHEM* **2003**, *631*, 209−223.
(59) Rovira, C.; Kunc, K.; Hutter, J.; Parrinello, M. *Inorg. Chem.* **2001**, *40*, 11−17.
(60) Jensen, K. P. *J. Phys. Chem. B* **2005**, *109*, 10505−10512.
(61) Stich, T. A.; Brooks, A. J.; Buan, N. R.; Brunold, T. C. *J. Am. Chem. Soc.* **2003**, *125*, 5897−5914.
(62) Stich, T. A.; Buan, N. R.; Brunold, T. C. *J. Am. Chem. Soc.* **2004**, *126*, 9735−9749.
(63) Schindler, O. *Helv. Chim. Acta* **1951**, *34*, 1356−1361.
(64) Bonnett, R.; Redman, D. G. *Proc. R. Soc. London, A* **1965**, *288*, 342−343.
(65) Fonseca Guerra, C. F.; Snijders, J. G.; te Velde, G.; Baerends, E. J. *Theor. Chem. Acc.* **1998**, *99*, 391−403.
(66) te Velde, G.; Bickelhaupt, F. M.; Baerends, E. J.; Fonseca Guerra, C. F.; van Gisbergen, S. J. A.; Snijders, J. G.; Ziegler, T. *J. Comput. Chem.* **2001**, *22*, 931−967.
(67) *ADF2004.01, SCM, Theoretical Chemistry*, Vrije Universeteit: Amsterdam, The Netherlands; http://www.scm.com.
(68) Fan, L.; Ziegler, T. *J. Chem. Phys.* **1992**, *96*, 9005−9012.
(69) Fan, L.; Ziegler, T. *J. Phys. Chem.* **1992**, *96*, 6937−6941.

depolarization ratios were calculated within the framework of time-dependent density functional response theory.[70,71] The absence of negative frequencies confirmed that the geometry optimizations had converged to true minima on the corresponding energy hypersurfaces.

A full DFT geometry optimization and frequency calculation were performed on a truncated model of Co^{1+}Cbl (Figure 1), in which all corrin ring substituents, including the nucleotide loop, were replaced with hydrogen atoms. A density functional composed of the Vosko, Wilk, and Nusair-5 (VWN-5) local density approximation (LDA) and the Perdew−Burke−Ernzerhof (PBE) generalized gradient approximation (GGA) exchange and correlation was utilized.[72,73] The same density functional was also applied to H_2O and the 5-coordinate Co^{1+}Cbl and Co^{2+}Cbi models. In both 5-coordinate models, the fifth ligand was an H_2O molecule in the lower axial position. To aid in the analysis of the computational results, vector representations of the normal modes for the truncated model of Co^{1+}Cbl were generated using the Jmol program.[74] A full geometry optimization was also performed on the complete Co^{1+}Cbi cofactor, in which the nucleotide loop is clipped off at the phosphodiester bond (Figure 1). In this calculation, the integration parameter was increased to 5.0 and the convergence criteria were loosened to: 0.001 Hartree in the total energy, 0.01 Hartree/Å in the Cartesian gradients, and 0.01 Å in the estimated uncertainty of the Cartesian coordinates. Additional computational geometries and frequencies not discussed in the main text are described in the Supporting Information.

Thermodynamic Properties. The standard Gibbs free energy for the gas-phase reaction between Co^{1+}Cbl and H_2O to produce 5-coordinate Co^{1+}Cbl was calculated at 298.15 K using a standard-state convention of 1 atm. The thermodynamic corrections were determined within the ideal gas approximation from the harmonic frequencies of the truncated models. Additionally, a PBE DFT single-point calculation for a 5-coordinate Co^{1+}Cbl model was performed by using the optimized 5-coordinate Co^{2+}Cbi geometry to assess the reorganization energy of 5-coordinate Co^{1+}Cbl following the reduction of 5-coordinate Co^{2+}Cbi.

Single-Point DFT and TDDFT Calculations. The ORCA 2.4.02 software package, developed by Dr. Frank Neese (MPI Mülheim, Germany),[75] was used to perform single-point DFT and TDDFT calculations on the truncated model of Co^{1+}Cbl using the Perdew-Wang LDA and the PBE GGA with the TZVP basis set for Co and the DGauss (Gaussian polarized double-ζ valence orbital) basis set for all other atoms.[73,76−78] The resolution of the identity (RI) approximation was used to speed up the calculation of the Coulomb terms within the molecule's charge distribution, as approximated using the Demon/J auxiliary basis set.[78,79] A total of 60 excited states were computed with TDDFT by including all single excitations between molecular orbitals (MOs) with orbital energies between −3 and +3 Hartrees using the RI and Tamm−Dancoff approximations.[80]

To facilitate the interpretation of the computational results, isosurface plots of the MOs and electron density difference maps (EDDMs) were generated with the gOpenMol program using isodensity values of 0.03 and 0.003 au, respectively.[81−83] Additionally, Abs traces were computed from the TDDFT results using a Gaussian convolution function with a bandwidth of 1250 cm^{-1} for each predicted transition to ease comparison with our experimental Abs data.[75] Results from additional single-point DFT and TDDFT calculations, including those performed on the core of the complete Co^{1+}Cbi geometry, are provided in the Supporting Information.

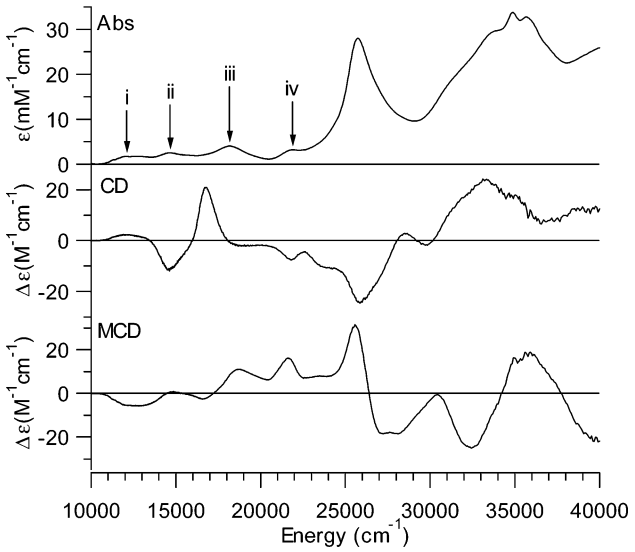

Figure 3. Abs, CD, and 7 T MCD spectra of Co^{1+}Cbl in a fluid 60:40 mixture of glycerol and NH_4Cl(aq) at 250 K. The four low-energy Abs features in the near-IR/visible region are labeled i−iv.

III. Results and Analysis

Electronic Spectroscopy. The Abs spectrum of Co^{1+}Cbl is characterized by a very intense, relatively sharp feature at 26 000 cm^{-1} and at least four significantly weaker bands in the near-IR/visible region centered at 12 500, 15 000, 18 000, and 22 000 cm^{-1} (Figure 3, top). The lack of any discernible features in the Abs, CD, and MCD spectra below 10 000 cm^{-1} suggests that band i corresponds to the lowest-energy electronic transition of Co^{1+}Cbl carrying significant Abs intensity. This feature, as well as Abs bands ii and iv, each appear to arise from a single electronic transition based upon their similar peak positions and band shapes in all three data sets. In contrast, Abs band iii clearly possesses contributions from at least two separate electronic transitions, because in the MCD spectrum, the corresponding feature is blue-shifted by ∼600 cm^{-1}. Similarly, at least two separate electronic transitions contribute to the dominant Abs feature at 26 000 cm^{-1}, as revealed by the presence of a derivative-shaped pseudo-A term in this region of the MCD spectrum. A number of additional spectral features are apparent toward higher energy, including a pair of relatively prominent Abs bands centered at ∼35 000 cm^{-1}.[52] Generally, when compared to the lower-energy region, the features above 25 000 cm^{-1} are significantly more intense in the Abs spectrum than in the CD and MCD spectra. On the basis of this observation and their high absolute Abs intensities, we attribute these features to corrin-centered $\pi \rightarrow \pi^*$ transitions.

Vibrational Spectroscopy. The high-energy regions of the rR spectra of Co^{1+}Cbl obtained with 514.5 and 454.5 nm

(70) van Gisbergen, S. J. A.; Snijders, J. G.; Baerends, E. J. *Comput. Phys. Commun.* **1999**, *118*, 119−138.
(71) van Gisbergen, S. J. A.; Snijders, J. G.; Baerends, E. J. *Chem. Phys. Lett.* **1996**, *259*, 599−604.
(72) Vosko, S. H.; Wilk, L.; Nusair, M. *Can. J. Phys.* **1980**, *58*, 1200−1211.
(73) Perdew, J. P.; Burke, K.; Ernzerhof, M. *Phys. Rev. Lett.* **1996**, *77*, 3865−3868.
(74) *Jmol 9.0*, www.jmol.org.
(75) Neese, F. *ORCA-An ab initio, Density Functional, and Semiempirical Program Package, Version 2.4, revision 2, July 2004*, Max-Planck-Institut fur Bioanorganische Chemie: Mulheim, Germany, 2004.
(76) Perdew, J. P.; Wang, Y. *Phys. Rev. B: Condens. Matter* **1992**, *45*, 13244−13249.
(77) Schäfer, A.; Huber, C.; Ahlrichs, R. *J. Chem. Phys.* **1994**, *100*, 5829−5835.
(78) Godbout, N.; Salahub, D. R.; Andzelm, J.; Wimmer, E. *Can. J. Chem.* **1992**, *70*, 560−571.
(79) Neese, F. *J. Comput. Chem.* **2003**, *24*, 1740−1747.
(80) Neese, F.; Olbrich, G. *Chem. Phys. Lett.* **2002**, *362*, 170−178.
(81) Laaksonen, L. *J. Mol. Graphics* **1992**, *10*, 33−34.
(82) Bergman, D. L.; Laaksonen, L.; Laaksonen, A. *J. Mol. Graphics Modell.* **1997**, *15*, 301−306.
(83) Laaksonen, L. *gOpenMol version 2.32*, Center for Scientific Computing: Espoo, Finland.

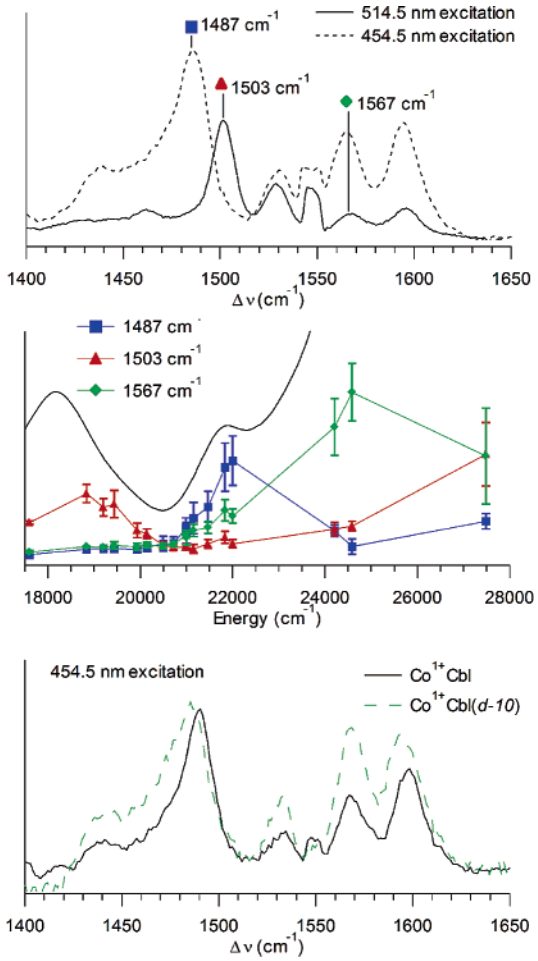

Figure 4. (Top) rR spectra of Co^{1+}Cbl at 77 K obtained with 514.5 and 454.5 nm (19 436 and 22 002 cm^{-1}, respectively) laser excitation. (Middle) Abs spectrum of Co^{1+}Cbl at 250 K (solid line) and 77 K rR excitation profile data for the corrin ring modes at 1487, 1503, and 1567 cm^{-1}. (Bottom) rR spectra of Co^{1+}Cbl and Co^{1+}Cbl(*d-10*) at 77 K obtained with 454.5 nm (22 002 cm^{-1}) excitation.

Table 1. Raman Shifts and Standard Deviations for Major Corrin Modes in Co^{1+}Cbl and Co^{1+}Cbl(*d-10*)

Co^{1+}Cbl	Co^{1+}Cbl (*d-10*)	$\Delta\Delta\nu$ (cm^{-1})
1487 ± 1.7 cm^{-1}	1483 ± 1.0 cm^{-1}	−4 cm^{-1}
1503 ± 1.7 cm^{-1}	1501 ± 1.0 cm^{-1}	−2 cm^{-1}
1530 ± 1.7 cm^{-1}	1529 ± 1.0 cm^{-1}	−1 cm^{-1}
1567 ± 2.3 cm^{-1}	1565 ± 1.0 cm^{-1}	−2 cm^{-1}
1595 ± 1.8 cm^{-1}	1590 ± 1.0 cm^{-1}	−5 cm^{-1}

(19 436 and 22 002 cm^{-1}, respectively) laser excitation are shown in Figure 4. The Raman shifts of the dominant features (summarized in Table 1), all of which correspond to corrin-based vibrational modes, are in good agreement with those reported previously.[53,54] Strikingly, though, the 1487 cm^{-1} mode that dominates the rR spectrum obtained with 454.5 nm excitation (Figure 4, top) was not previously observed. Presumably, this mode was overlooked in the past due to its negligible rR enhancement for 514.5 nm excitation and the fact that the corresponding region was not analyzed in detail when 457.9 nm excitation was used. Because rR spectra of Co^{2+}Cbl also exhibit an intense feature at 1487 cm^{-1},[62] additional experiments were performed to explore the possibility that our samples were only partially reduced to the Co^{1+}Cbl state. The rR enhancement behaviors of the 1487 cm^{-1} modes of Co^{1+}Cbl and Co^{2+}Cbl were found to be significantly different; i.e., whereas for Co^{2+}-Cbl maximum enhancement of this mode occurs at 20986 cm^{-1}, which roughly coincides with the peak position of the dominant feature in the corresponding Abs spectrum,[62] for Co^{1+}Cbl, this mode is most strongly enhanced with 22 002 cm^{-1} excitation (Figure 4, middle), close to the peak position of Abs band iv (Figure 2). This result demonstrates that both Co^{1+}Cbl and Co^{2+}-Cbl possess corrin-based vibrational modes with a frequency of 1487 cm^{-1}.

Replacement of the hydrogen attached to C_{10} of the corrin ring (Figure 1) by a deuterium atom causes all of the features between 1480 and 1600 cm^{-1} in the rR spectra of Co^{1+}Cbl to downshift to some degree (Figure 4, bottom and Table 1), corroborating their assignment as corrin-based normal modes of vibrations. The most pronounced shifts are expected for modes that involve large nuclear motions of C_{10}, in particular the totally symmetric stretching mode polarized along the short axis (SA, coincident with Co···C_{10} vector in Figure 1) of the corrin ring as judged from a previous study of MeCbl.[84] In the case of Co^{1+}Cbl, the 1487 and 1595 cm^{-1} modes exhibit the largest shifts upon H → D exchange at C_{10} (Table 1). On the basis of this observation and the fact that the frequency of the SA stretch appears to downshift uniformly with decreasing positive charge on the Co center, from 1543 cm^{-1} for H_2OCbl^{+}[61] to 1542 cm^{-1} for MeCbl[61] and 1508 cm^{-1} for Co^{2+}Cbl,[62] it is reasonable to assign the 1487 cm^{-1} feature in the rR spectra of Co^{1+}Cbl (Figure 4) to the SA stretching mode.

Of the five corrin-based modes listed in Table 1, those at 1487, 1503, and 1567 cm^{-1} show the most dramatic rR enhancement; their excitation profiles are displayed in Figure 4 (middle). The SA stretch at 1487 cm^{-1} is predominantly enhanced for excitation in resonance with Abs band iv, which suggests that the corresponding transition is short-axis polarized. The rR excitation profile of the 1503 cm^{-1} mode is complementary to that of the SA stretch, peaking in close proximity to Abs band iii and the high-energy side of the dominant Abs feature. The frequency of this mode is only moderately affected by H → D exchange at C_{10} (Table 1) and falls within a range where the long-axis (LA, coincident with C_5···C_{15} vector in Figure 1) polarized totally symmetric stretching mode of the corrin ring is expected to occur based on a comparison with H_2OCbl^{+} (1499 cm^{-1}) and MeCbl (1490 cm^{-1}).[61] Consequently, the 1503 cm^{-1} mode of Co^{1+}Cbl is attributed to the LA stretch, which implies that the electronic transitions responsible for Abs band iii and the broadening of the dominant Abs feature on its high-energy side are long-axis polarized. To identify the origin of the 1567 cm^{-1} mode that shows a dramatic enhancement for laser excitation near 24 000 cm^{-1}, as well as to obtain quantitative descriptions for all other modes including the 1530 and 1595 cm^{-1} modes which show minimal resonance enhancement over the range of excitation wavelengths utilized, a DFT-based vibrational analysis was carried out for a suitably truncated Co^{1+}Cbl model (vide infra).

Gaussian Deconvolution of Electronic Spectra. The Gaussian deconvolution of our Abs, CD, and MCD spectra indicates that at least 12 electronic transitions contribute to the region below 30 000 cm^{-1} (Figure 5, Table 2). Closer analysis of the three data sets, in particular the relative peak positions and their

(84) Puckett, J. M.; Mitchell, M. B.; Hirota, S.; Marzilli, L. G. *Inorg. Chem.* **1996**, *35*, 4656−4662.

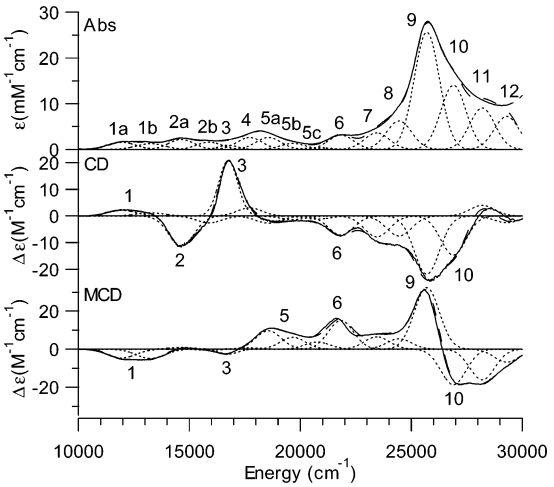

Figure 5. Gaussian deconvolutions of the Abs, CD, and 7 T MCD spectra of Co^{1+}Cbl in a fluid 60:40 mixture of glycerol and NH_4Cl(aq) at 250 K. The solid lines show the experimental data, the dotted lines show the individual Gaussian peaks simulated using the fit parameters in Table 2, and the dashed lines show the sums of the individual Gaussian peaks.

Table 2. Fit Parameters from the Gaussian Deconvolutions of the Abs, CD, and MCD Spectra of Co^{1+}Cbl in Figure 5

peak	energy (cm^{-1})	ϵ(Abs) ($mM^{-1}cm^{-1}$)	$\Delta\epsilon$(CD) ($M^{-1}cm^{-1}$)	$\Delta\epsilon$(MCD) ($M^{-1}cm^{-1}$)	width (cm^{-1})
1a	11 950	1.55	2.15	−4.65	900
1b	13 250	1.26	1.21	−4.95	900
2a	14 640	2.21	−11.32	0.91	800
2b	15 890	1.58	−2.58	−0.50	800
3	16 750	0.92	20.80	−2.63	600
4	17 715	2.60	3.03	0.69	800
5a	18 565	2.61	−2.70	9.70	800
5b	19 665	1.30	−1.31	6.20	800
5c	20 765	0.41	−1.14	3.74	800
6	21 830	3.15	−7.15	15.05	800
7	23 450	3.61	−7.80	6.45	800
8	24 450	6.24	−7.48	5.40	800
9	25 700	25.64	−21.79	32.33	800
10	26 900	14.03	−14.65	−18.68	800
11	28 200	9.07	3.99	16.14	800
12	29 300	7.23	−2.48	−6.82	800

signs in the CD and MCD spectra, reveals that 3 of these 12 transitions exhibit some vibronic structure with a partially resolved progression in a corrin-based normal mode, i.e., transition 1 (spacing of 1300 cm^{-1}), 2 (1250 cm^{-1}), and 5 (1100 cm^{-1}).[85] In each case, the electronic origin is the most intense member of the vibrational progression, indicating that the corresponding Huang−Rhys parameter is <1. Note that a similar vibronic structure is generally observed for the intense lowest-energy Abs feature of Co^{3+}Cbls (the so-called α,β region) that arises from the corrin-based HOMO → LUMO (i.e., $\pi \rightarrow \pi^*$) transition.[61]

Consistent with the qualitative analysis of the Co^{1+}Cbl Abs, CD, and MCD spectra presented above, the results from our Gaussian deconvolution indicate that Abs bands i, ii, and iv (corresponding to peaks 1, 2, and 6, respectively, in Figure 5) are due to single electronic transitions, whereas Abs band iii (peaks 4 and 5) has contributions from two distinct electronic transitions.[86] They reveal further that the pseudo-A term in the MCD spectrum near 26 000 cm^{-1} originates from two oppositely signed B terms, one corresponding to peak 9 that dominates the Abs spectrum in this region and the other to peak 10, which is responsible for the broadening of this Abs feature on its high-energy side and for the weak shoulder in the CD spectrum. The MCD spectrum therefore provides conclusive evidence that the asymmetry of the dominant Abs feature is due to the presence of two distinct electronic transitions contributing to this region rather than a vibrational progression associated with a single transition.

The Gaussian deconvolution also aids in deciphering some more subtle features of the Abs, CD, and MCD spectra of Co^{1+}-Cbl. Although transition 3 is the least intense contributor to the Abs spectrum of Co^{1+}Cbl, it produces one of the most intense features in the CD spectrum, indicating that this transition possesses significant magnetic dipole character and relatively little electric dipole character. Peaks 7 and 8 are difficult to discern directly in the Abs, CD, and MCD spectra because they are obscured by peak 9, but they are clearly needed in our spectral deconvolution to obtain a satisfactory fit of the experimental data.

Table 3. Co−N Bond Lengths and Corrin Fold Angles Along the $C_5\cdots C_{15}$ Vector (θ) and Along the $Co\cdots C_{10}$ Vector (ϕ) for the PBE DFT-Optimized, Truncated CO^{1+}Cbl Model and the PBE DFT-Optimized, Complete Co^{1+}Cbi Model

	truncated	complete
$Co-N_A$	1.840 Å	1.831 Å
$Co-N_B$	1.909 Å	1.917 Å
$Co-N_C$	1.907 Å	1.898 Å
$Co-N_D$	1.840 Å	1.845 Å
θ(LA)	7.3°	10.6°
ϕ(SA)	4.4°	6.8°

DFT Geometry Optimizations and Frequency Calculations. In the DFT-optimized, truncated model of Co^{1+}Cbl obtained with the PBE functional, the corrin macrocycle is nearly planar and the Co−N bond lengths vary between 1.84 and 1.91 Å (Table 3), in excellent agreement with the average Co−N bond lengths of 1.86 and 1.88 Å obtained in two recent XAS studies.[8,9] The highest occupied molecular orbital (HOMO) is predicted to be Co $3d_{z^2}$-based, as expected on the basis of simple ligand-field theory considerations. The ground state is therefore a closed-shell $3d^8$ singlet, which was also verified in unrestricted calculations. In contrast, a previous computational study using the B3LYP hybrid density functional, a different approximation to the true density functional, concluded that Co^{1+}Cbl possesses an open-shell, antiferromagnetically coupled Co $3d^7$/corrin radical ground state.[56] However, the prediction of a closed-shell d^8 singlet by our computations is supported by the fact that this configuration was found to produce the dominant (67%) contribution to the CASPT2 multi-configurational ground-state wave function obtained in a previous computational study on a truncated Co^{1+}Cbl model.[60] Also note that the TDDFT computational results presented in the next section strongly suggest that the closed-shell d^8 singlet description for Co^{1+}Cbl is correct.

To test computationally the widely accepted assumption that Co^{1+}Cbl is a 4-coordinate species, we added an H_2O molecule

(85) Although our MCD data may seem inconsistent with the assignment of peaks 2a and 2b as members of a vibrational progression because they appear to be oppositely signed, it should be noted that these features are extremely weak in the MCD spectrum and thus their signs cannot be established with certainty.

(86) Note that peaks 4 and 5 are not members of a vibrational progression with S > 1, as they appear as oppositely signed features in the CD spectrum.

at 2.2 Å from the Co center to the lower axial position of our truncated Co^{1+}Cbl model and re-optimized the geometry. The H_2O molecule moved away from Table 3. Co−N bond lengths and corrin fold angles along the $C_5\cdots C_{15}$ vector (θ) and along the $Co\cdots C_{10}$ vector (ϕ) for the PBE DFT-optimized, truncated Co^{1+}Cbl model and the PBE DFT-optimized complete Co^{1+}-Cbi model the corrinoid and rotated so as to position one of its H atoms ~2.4 Å below the strongly nucleophilic Co atom. Thus, in a vacuum, H_2O is expected to weakly coordinate to Co^{1+}-Cbl through one of its H atoms rather than its O atom. However, this complex is predicted to be unstable toward decomposition into H_2O and 4-coordinate Co^{1+}Cbl, as the standard Gibbs free energy for the decomposition reaction is −1.96 kcal/mol in vacuo and presumably even more negative in aqueous solution (Table S2). This prediction is consistent with an electrochemical study of vitamin B_{12} derivatives, which revealed that the maximum lifetime of a 5-coordinate Co^{1+}Cbl complex at room temperature is shorter than 10^{-4}−10^{-5} s.[87]

To assess the influence of the methyl groups and side-chains on the Co^{1+}Cbl geometry (Figure 1), these groups, with the exception of the nucleotide loop and the DMB base, were appended to the DFT-optimized, truncated Co^{1+}Cbl species to generate a complete model of Co^{1+}Cbi, a Co^{1+}Cbl derivative that is spectroscopically indistinguishable from, but computationally more accessible than, the actual cofactor.[52] This Co^{1+}-Cbi model was then geometry-optimized using the PBE density functional. Inspection of Table 3 reveals that the addition of the side chains to the truncated model has virtually no effect on the average Co−N bond length and causes only a slight increase in the fold angles. This result indicates that the folding of the corrin ring in Co^{1+}Cbl is almost entirely controlled by the portion of the cofactor included in the truncated model of Co^{1+}Cbl used in our DFT computations.

A major advantage of our truncated Co^{1+}Cbl model over the complete Co^{1+}Cbi model is that it is sufficiently small to permit DFT-based vibrational frequency calculations, which can be used to verify that the geometry-optimization converged to a true minimum on the potential energy hypersurface and to assist in the analysis of vibrational spectra. Because the experimental rR spectra of Co^{1+}Cbl are dominated by corrin-based modes between 1475 and 1650 cm^{-1} (Figure 4), the following analysis of the DFT-predicted Raman spectra (Figures 6 and S4) is restricted to this frequency range. As indicated in Figure 6 (top), the frequency of the SA stretch is computed at 1484 cm^{-1} with a predicted downshift upon H → D exchange at C_{10} of 7 cm^{-1}, strongly supporting our assignment of the 1487 cm^{-1} feature in the experimental rR spectra of Co^{1+}Cbl, which downshifts by 4 cm^{-1} in Co^{1+}Cbl(*d-10*) (Table 1), to this mode. Although the SA stretch is predicted to have negligible off-resonance intensity, it is expected to be strongly resonance enhanced by coupling to certain electronic transitions due to its totally symmetric character, as revealed by the low computed depolarization ratio of 0.20 (Figure 6). Again, this prediction concurs nicely with our experimental rR data; i.e., whereas the 1487 cm^{-1} mode is very prominent in the rR spectrum obtained with 454.5 nm laser excitation, it carries negligible "off-resonance" intensity in the spectrum recorded with 514.5 nm excitation (Figure 4, top).

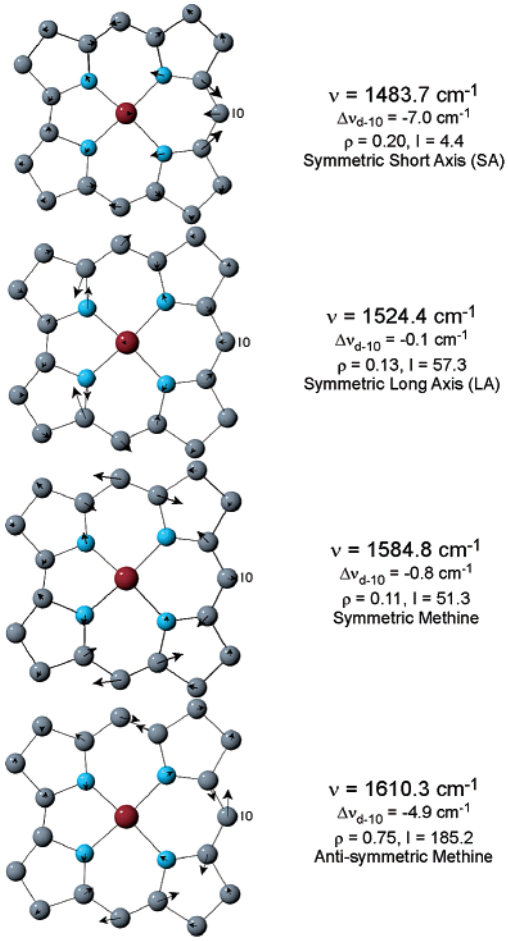

Figure 6. PBE DFT-computed eigenvector representations of the relevant corrin-based stretching modes for Co^{1+}Cbl. Their computed frequencies (ν), downshifts in response to H → D exchange at C_{10} ($\Delta\nu_{d-10}$), depolarization ratios (ρ), and off-resonance Raman intensities (I) are shown on the right.

The DFT-computed frequencies for the symmetric LA and methine stretches are 1524 and 1585 cm^{-1}, respectively, and the antisymmetric methine stretch is predicted at 1610 cm^{-1} (Figure 6). Although minimal shifts for H → D exchange at C_{10} are predicted for the former two modes, a 5 cm^{-1} downshift is computed for the antisymmetric methine stretch. On the basis of a comparison of these computational results with our experimental rR data (Table 1), we assign the two features at 1503 and 1567 cm^{-1} in our experimental spectra (Figure 4, top) to the symmetric LA and methine stretches, respectively, and the 1595 cm^{-1} feature to the antisymmetric methine stretch. As indicated in Figure 6, both the symmetric LA and methine stretching modes are predicted to carry relatively little off-resonance Raman intensity and to possess low depolarization ratios, consistent with our rR excitation profiles obtained for the 1503 and 1567 cm^{-1} modes (Figure 4, middle) that clearly require these vibrations to be totally symmetric in character due to their strong coupling to electronic transitions. Alternatively, the antisymmetric methine stretching mode is predicted to carry significant off-resonance Raman intensity and possess a high depolarization ratio of 0.75 (Figure 6), which also concurs nicely with our rR excitation profile data, as the 1595 cm^{-1} mode shows minimal rR enhancement over the entire excitation wavelength range investigated (Figure S3).

(87) Faure, D.; Lexa, D.; Saveant, J. M. *J. Electroanal. Chem.* **1982**, *140*, 285−295.

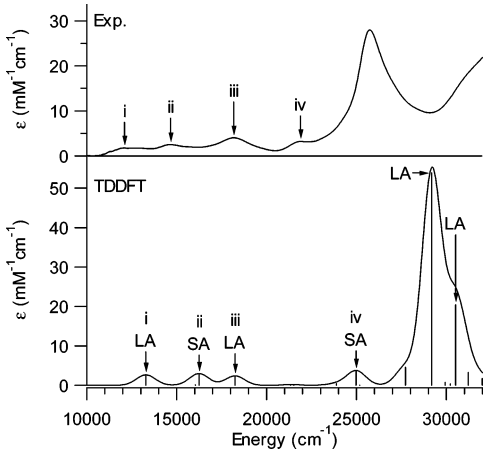

Figure 7. (Top) Abs spectrum of Co^{1+}Cbl in a fluid 60:40 mixture of glycerol and NH_4Cl(aq) at 250 K. (Bottom) PBE TDDFT-computed Abs spectrum and transition polarizations for the PBE DFT-optimized truncated model of Co^{1+}Cbl.

Whereas the computed frequency for the symmetric SA stretch of 1484 cm^{-1} is in excellent agreement with the experimental value of 1487 cm^{-1}, the frequencies for the symmetric LA and methine stretches as well as for the antisymmetric methine stretch are overestimated by 21, 18, and 15 cm^{-1}, respectively. This result can be understood on the basis of the truncation scheme employed to generate the Co^{1+}Cbl model used in our frequency calculation. As all of the corrin normal modes under discussion primarily involve nuclear displacements within the plane of the macrocycle, the effective masses, and thus the frequencies, associated with these modes may be modulated by substituents attached to the periphery of the corrin ring. Among those, the two methyl groups at C_5 and C_{15} (Figure 1) are the only substituents located within the corrin ring plane that are not included in our truncated Co^{1+}Cbl model. Because these methyl groups are modeled by hydrogen atoms, our computation overestimates the frequencies of the corrin-based normal modes involving a significant movement of the C_5 and/or C_{15} carbons, which includes the symmetric LA and methine stretches as well as the anti-symmetric methine stretch, but not the symmetric SA stretch (Figure 6).

TDDFT Computational Results. The TDDFT-computed Abs spectrum for the DFT-optimized, truncated Co^{1+}Cbl model is in excellent agreement with the experimental Abs spectrum with respect to band positions and relative intensities (Figure 7).[88] In the TDDFT-computed spectrum, four weak features are predicted in the visible/near-IR region along with a considerably more intense, relatively sharp band at higher energy. This latter band has three main contributors, including one dominant transition that is bracketed by a pair of weaker transitions. Notably, a similar set of three transitions contributes to the dominant feature in the experimental Abs spectrum, as revealed by our Gaussian deconvolution (Figure 5 and Table 2, peaks 8−10).

In addition to properly predicting the number, energies, and relative intensities of the major features in the Co^{1+}Cbl Abs spectrum, the TDDFT computation also yields transition polarizations that agree well with those determined experimentally on the basis of our rR excitation profile data (Figure 4).

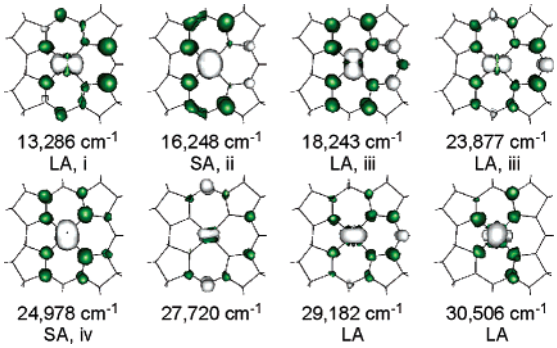

Figure 8. PBE TDDFT-computed EDDMs and polarizations for selected electronic transitions, obtained using the PBE DFT-optimized truncated model of Co^{1+}Cbl. Gray/green indicate loss/gain of electron density.

Electronic transitions polarized along the short axis of the corrin ring ($Co\cdots C_{10}$ vector, Figure 1) should give rise to predominant rR enhancement of the symmetric SA stretch at 1487 cm^{-1}.[61] Alternatively, electronic transitions polarized along the long axis ($C_5\cdots C_{15}$ vector) should primarily enhance the symmetric LA stretch at 1503 cm^{-1}. Hence, the rR excitation profiles for the symmetric SA and LA stretches indicate that the transition responsible for the Abs feature at ∼22 000 cm^{-1} (peak 6 in Figure 5) is short-axis polarized, whereas those associated with the features at 16 000 and 27 000 cm^{-1} (peaks 4/5 and 10, respectively) are long-axis polarized, in excellent agreement with the TDDFT predicted polarizations (Figure 7).

Because the strong rR enhancement of the symmetric methine stretch at 1567 cm^{-1} for excitation near the dominant Abs feature (Figure 4, middle) cannot be correlated directly with the polarization(s) of the corresponding transition(s), electron density difference maps (EDDMs) were computed for relevant electronic excited states to allow for a visual analysis of changes in the electron density upon electronic excitation (Figure 8). On the basis of the calculated normal mode description for the symmetric methine stretch (Figure 6), this mode should be rR enhanced primarily upon excitation in resonance with electronic transitions that cause large changes in electron density at C_5, C_6, C_{14}, and C_{15}. The EDDM associated with the TDDFT-computed excited state at 27 720 cm^{-1} reveals particularly large electron-density changes at these four carbon atoms. Hence, excitation in resonance with the corresponding transition in the experimental spectrum (peak 8, Figure 5) should give rise to strong rR enhancement of the symmetric methine stretch, which is indeed the case (Figure 4, middle).

TDDFT-Assisted Spectral Assignments. In light of the fact that the TDDFT-computed Abs spectrum for our Co^{1+}Cbl model agrees well with our Abs and rR spectroscopic data, it is reasonable to use the DFT-computed MO descriptions as the basis for assigning key spectral features in the experimental Abs spectrum. Isosurface plots for the relevant frontier MOs of the DFT-optimized, truncated Co^{1+}Cbl model are shown in Figure 9.[89] These MOs have been designated according to their transformation behavior in the approximate C_{2v} molecular point group, with the pseudo-C_2 axis oriented along the short axis (defined here as the **x**-axis to preserve the d-orbital labels commonly used for square planar complexes), the **y**-axis coinciding with the long axis, and the **z**-axis being perpendicular

(88) The TDDFT-computed Abs spectrum for the core of the complete Co^{1+}-Cbi model is nearly identical (Figure S5).

(89) Nearly identical results were obtained for the core of the complete Co^{1+}-Cbi model (Figure S13).

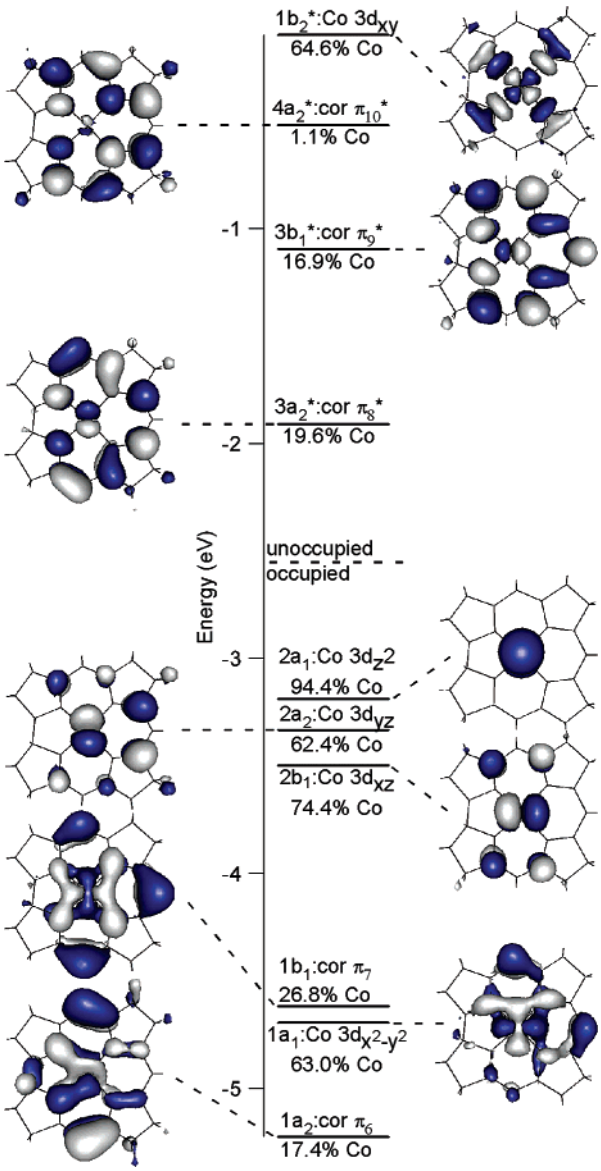

Figure 9. Isosurface plots of the PBE DFT-computed MOs, with the approximate C_{2v} symmetry labels and percent contributions from the Co 3d orbitals, for the PBE DFT-optimized truncated model of Co^{1+}Cbl.

to the plane of the corrin ring. The relative energies of the five Co 3d-based MOs are as expected for a nearly square planar complex with a strongly σ- and weakly π-donating tetradentate ligand; i.e., the Co $3d_{x^2y^2}$-derived MO is lowest in energy because it is essentially nonbonding, whereas the strongly σ-antibonding $3d_{xy}$-derived MO is highest in energy and thus remains unoccupied. Moreover, consistent with the "supernucleophilic" nature of Co^{1+}Cbl, our computations predict that the HOMO has primarily Co $3d_{z^2}$ orbital character.

The highest-energy corrin π-based occupied MO, which we designate cor π_7 to specify that the corrin π system contains 14 electrons distributed over seven different MOs ($\pi_1-\pi_7$), is nearly 1.5 eV lower in energy than the Co $3d_{xz}$-, $3d_{yz}$-, and $3d_{z^2}$-based orbitals. Because of this relative energy ordering of the occupied frontier MOs and the fact that the three lowest-energy unoccupied MOs are all cor π^*-based ($\pi_8^*-\pi_{10}^*$), Co 3d → cor π^* charge transfer (CT) transitions are expected to occur at lower energies than cor π → cor π^* and Co 3d → Co 3d transitions. However, to correlate individual features in the experimental Abs spectrum with specific electronic transitions, a more detailed analysis of the TDDFT results is required.

Table 4. PBE TDDFT-Computed Energies, Oscillator Strengths (f), Dominant (>10%) One-Electron Excitations, Polarizations in the Corrin Plane within 2° of Either the SA or LA of the Corrin Ring, and Approximate C_{2v} Symmetry Labels for the 15 Lowest-Energy Excited States of the PBE DFT-Optimized, Truncated Model of Co^{1+}Cbl

E(cm^{-1})	f	%	donor	acceptor	notes	peak[a]
9459	0.00006	96%	d_{z^2}	cor π_8^*	SA, A_2	
13 286	0.01523	91%	d_{xz}	cor π_8^*	LA, B_2	1
16 038	0.00057	94%	d_{z^2}	cor π_9^*	B_1	3
16 248	0.01665	25% 60%	d_{xz} d_{yz}	cor π_9^* cor π_8^*	SA, A_1	2
18 243	0.01381	84%	d_{yz}	cor π_9^*	LA, B_2	4 or 5
21 335	0.00092	34% 17% 36%	$d_{x^2-y^2}$ cor π_7 d_{z^2}	cor π_8^* cor π_8^* cor π_{10}^*		
21 510	0.00013	19% 11% 60%	$d_{x^2-y^2}$ cor π_7 d_{z^2}	cor π_8^* cor π_8^* cor π_{10}^*		
23 877	0.00244	17% 28% 53%	$d_{x^2-y^2}$ cor π_7 d_{xz}	cor π_8^* cor π_8^* cor π_{10}^*	LA	4 or 5
24 978	0.02109	16% 68%	d_{xz} d_{yz}	cor π_9^* cor π_{10}^*	SA, A_1	6
25 182	0.00038	22% 61%	$d_{x^2-y^2}$ d_{yz}	cor π_9^* d_{xy}	SA, B_1	
27 720	0.02651	27% 24% 12%	cor π_6 cor π_7 d_{xz}	cor π_8^* cor π_9^* cor π_9^*	A_1	7 or 8
29 182	0.31067	25% 34% 18%	cor π_7 d_{xz} d_{z^2}	cor π_8^* cor π_{10}^* d_{xy}	LA, B_2	9
29 925	0.00418	12% 14% 25% 17%	cor π_6 d_{x^2} d_{xz_2} d_{z^2}	cor π_8^* cor π_9^* d_{xy} Co 4s		
30 216	0.00198	17% 46%	cor π_6 d_{xz}	cor π_8^* d_{xy}		
30 506	0.11778	49%	d_{z^2}	d_{xy}	LA, B_2	10

[a] Assignments for the Gaussian-resolved peaks in the experimental Abs spectrum (Figure 5).

In the TDDFT approach, each electronic transition is expressed in terms of a linear combination of fractional one-electron excitations (Table 4). In the approximate C_{2v} molecular point group, transitions from the ground state (A_1 symmetry) to excited states of A_1 and B_2 symmetries are electric dipole allowed for light polarized with the electric field vector **E** oriented along the corrin ring's short and long axes, respectively. Although transitions to excited states of B_1 symmetry are also electric-dipole allowed, for light polarized with **E** oriented perpendicular to the corrin ring plane, these transitions should be much weaker because of the nearly planar structure of Co^{1+}-Cbl. Similarly, transitions to excited states of A_2 symmetry should carry little Abs intensity because they are formally electric-dipole forbidden.

The five lowest-energy TDDFT-computed transitions, which occur between 9000 and 20 000 cm^{-1}, primarily involve one-electron excitations from the Co $3d_{xz}$-, $3d_{yz}$-, and $3d_{z^2}$-based occupied MOs to the cor π_8^*- and π_9^*-derived unoccupied MOs (Table 4) and, thus, formally correspond to Co 3d → cor π^* CT transitions. However, as revealed by the corresponding

EDDMs (Figure 8), these transitions also possess substantial cor $\pi \rightarrow \pi^*$ character due to the covalent mixing between the Co 3d and corrin π/π^* orbitals. By combining the information gained from our spectral deconvolutions and rR excitation profile analysis for Co^{1+}Cbl (vide supra), a one-to-one correlation between most of the TDDFT-predicted and experimentally observed transitions in this region can be established, as indicated in the last column of Table 4. Consistent with the C_{2v} selection rules outlined above, the SA and LA polarized transitions to excited states of effective A_1 and B_2 symmetries, respectively, are considerably more intense than transitions involving B_1 and A_2 excited states. Nonetheless, the **z**-polarized Co $3d_{z^2} \rightarrow$ cor π_9^* transition (B_1 excited state) is likely responsible for the appearance of peak 3, which is particularly prominent in the CD spectrum of Co^{1+}Cbl (Figure 5). Note that the narrower width of peak 3 relative to the other features (Table 2) indicates that the corresponding excited state is less strongly distorted, which is consistent with it being associated with a transition originating from the Co $3d_{z^2}$-based MO that has insignificant orbital contributions from the corrin ring.

The next set of TDDFT-computed transitions, which span the range from 20 000 to 25 000 cm^{-1}, primarily involve one-electron excitations from the Co $3d_{xz}$-, $3d_{yz}$-, and $3d_{z^2}$-based occupied MOs to the cor π_{10}^*-derived unoccupied MO, but also possess varying amounts of Co $3d_{x^2-y^2} \rightarrow$ cor π_8^* CT character (see Table 4 for details). Toward higher energy, the TDDFT-computed transition at 27 720 cm^{-1} is likely responsible for peak 7 or 8 in the experimental Co^{1+}Cbl spectra (Figure 5).[90] It is formally a corrin $\pi \rightarrow \pi^*$ transition, with similar contributions from the cor $\pi_6 \rightarrow$ cor π_8^* and cor $\pi_7 \rightarrow$ cor π_9^* one-electron excitations (Table 4). The isosurface plots associated with these four corrin π/π^*-based MOs (Figure 9) suggest that this transition will substantially weaken the $C_4 \cdots C_5 \cdots C_6$ and $C_{14} \cdots C_{15} \cdots C_{16}$ three-center π bonds, which provides a rationale for the strong rR enhancement of the symmetric methine stretch for laser excitation near peaks 7 and 8 (Figure 4, middle).

The TDDFT-predicted transition at 29 182 cm-1 has the highest computed intensity of all transitions and is therefore assigned to peak 9, which is the dominant contributor to the experimental Abs spectrum (Figure 5). This transition primarily involves the cor $\pi_7 \rightarrow$ cor π_8^* and Co $3d_{xz} \rightarrow$ cor π_{10}^* one-electron excitations, but also contains considerable Co $3d_{z^2} \rightarrow$ Co $3d_{xy}$ character (Table 4). This latter contribution is a direct reflection of the large electronic reorganization at the Co center that occurs in the corresponding excited state, which is particularly evident from the computed EDDM associated with this transition (Figure 8). Similarly, although the Co $3d_{z^2} \rightarrow$ Co $3d_{xy}$ one-electron excitation is predicted to be the principal contributor to the TDDFT-computed transition at 30 506 cm^{-1} (Table 4), which we assign to peak 10, the corresponding EDDM (Figure 8) clearly shows that this transition actually has predominant Co 3d $\rightarrow$ cor π^* CT character. In this case, a direct analysis of the TDDFT results is misleading, because a large number of additional one-electron excitations contribute to this transition, albeit by less than 10%. In the corresponding EDDM, all of these contributions are properly accounted for to reveal the true nature of this transition.

(90) The TDDFT-predicted transition energies for peaks 6−10 are overestimated by 3000−3500 cm^{-1}, which is probably due to the truncation scheme employed in generating our Co^{1+}Cbl model. Comparable deviations between TDDFT-computed and experimental transition energies were noted in previous studies of Co^{3+}- and Co^{2+}Cbl species using similarly truncated cofactor models.

IV. Discussion

Although the biologically active forms of vitamin B_{12}, AdoCbl and MeCbl,[61] and their one-electron reduced derivative, Co^{2+}Cbl,[62] have been studied extensively using a wide range of spectroscopic and computational methods, the geometric and electronic properties of the "superreduced" B_{12} cofactor, Co^{1+}-Cbl, have remained largely unexplored. In this study, we have used a combination of complementary spectroscopic tools to probe the ground and excited electronic states of Co^{1+}Cbl. Our Gaussian-deconvoluted Abs, CD, and MCD spectra, together with our rR excitation profile data, have provided an excellent framework for evaluating DFT and TDDFT electronic structure calculations. Using the PBE density functional for both ground- and excited-state computations, excellent agreement has been achieved between the experimental and computed frequencies of the corrin-based normal modes of vibration (Table 1 and Figure 6) as well as between the experimental and computed Abs spectra (Figure 7). Together, our spectroscopic and computational studies provide significant new insight into the geometric, vibrational, and electronic properties of the "superreduced" B_{12} cofactor. Below, key findings from these studies and their implications with respect to the reactivity of Co^{1+}Cbl are discussed, and spectroscopic trends along the series from Co^{3+}Cbls to Co^{2+}Cbl and Co^{1+}Cbl are explored.

Ground-State Properties of Co^{1+}Cbl. Our DFT-based geometry optimizations and thermodynamic analysis for the coordination of a water molecule to our 4-coordinate Co^{1+}Cbl model, along with the TDDFT results discussed in the next section, provide compelling evidence that the cobalt center in Co^{1+}Cbl is in a 4-coordinate, square-planar ligand environment. According to DFT calculations, no stationary state exists for 5-coordinate Co^{1+}Cbl with a Co−O bond, and the gas-phase complex containing a weak Co−H bond lies ∼2 kcal/mol higher in energy than the separated species. Thus, in aqueous solution, the axial H_2O ligand is predicted to dissociate from the Co center to participate in strong H-bonding with other solvent molecules.

In both DFT-optimized 4-coordinate Co^{1+}Cbl models, the average Co−N bond length is 1.87 Å (Table 3), in excellent agreement with the experimental values of 1.86 and 1.88 Å obtained in two independent EXAFS studies.[8,9] The LA fold along the $C_5 \cdots C_{15}$ vector of 7.3° in the truncated Co^{1+}Cbl model (Table 3) is significantly smaller than observed in the crystal structures of MeCbl and Co^{2+}Cbl, 14.7° and 16.3°, respectively.[1,6] This fold angle is only slightly increased to 10.6° in the complete Co^{1+}Cbi model (Table 3), suggesting that the planarity of our Co^{1+}Cbl model is due to electronic factors rather than the omission of the corrin ring side-chains. Presumably, the corrin ring in Co^{1+}Cbl adopts a relatively planar conformation to minimize the destabilization of the doubly occupied Co $3d_{z^2}$ MO, an orbital that is formally unoccupied and only singly occupied in MeCbl and Co^{2+}Cbl, respectively.[61,62]

Our DFT-assisted assignments of the corrin-based normal modes of vibration for Co^{1+}Cbl (Figure 6) can be compared with those established previously for MeCbl using the B3LYP scaled quantum mechanical (SQM) method,[91] as the conforma-

(91) Andruniow, T.; Zgierski, M. Z.; Kozlowski, P. M. *J. Phys. Chem. A* **2002**, *106*, 1365−1373.

tions of the corrin macrocycle are nearly identical for these two species. This structural similarity is reflected in the close resemblance of the 1400−1600 cm^{-1} region of the Co^{1+}Cbl and MeCbl Raman spectra,[61] a region that is dominated by corrin-based vibrational modes. The B3LYP SQM study of MeCbl predicted two symmetric corrin stretching modes in this energy window, at 1452 and 1497 cm^{-1}, which correspond to the SA and LA stretching modes of Co^{1+}Cbl as revealed by the close resemblance of the respective eigenvectors (Figure 6). In contrast, the symmetric and anti-symmetric methine stretches identified here for Co^{1+}Cbl, which involve the in-phase and out-of-phase combinations of the $C_4\cdots C_5\cdots C_6$ and $C_{14}\cdots C_{15}\cdots C_{16}$ stretching motions, respectively (Figure 6), do not have any direct counterparts in the B3LYP SQM computed Raman spectrum of MeCbl. Instead, in MeCbl, the $C_4\cdots C_5\cdots C_6$ and $C_{14}\cdots C_{15}\cdots C_{16}$ stretching motions are uncoupled, which results in two nearly degenerate, nontotally symmetric, normal modes. Consequently, these modes are unable to couple to electronic transitions, consistent with their insignificant enhancement in rR spectra obtained for MeCbl.[61]

Excited-State Properties of Co^{1+}Cbl. The key features in the Co^{1+}Cbl Abs spectrum had already been assigned on the basis of B3LYP TDDFT and CASPT2 computations;[58,60] however, these assignments were hampered by the fact that much of the information obtained from the Gaussian deconvolution of the Abs, CD, and MCD spectra performed in this work (Figure 5, Table 2), as well as the polarization information from the rR profile data (Figure 4), had not previously been available. Inspection of the EDDMs associated with the dominant transitions in the PBE TDDFT-computed Abs spectrum (Figure 8) reveals that the four moderately intense features below 25 000 cm^{-1} in the experimental Co^{1+}Cbl Abs spectrum (Figure 7) arise from Co 3d → cor π^* CT transitions. Alternatively, the dominant Abs band centered at 26 000 cm^{-1} originates from a transition with predominant cor π → cor π^* character, where the MOs derived from the HOMO and LUMO of the free corrin ring (cor π_7 and cor π_8^*, respectively, Figure 9) serve as the principal contributors. Qualitatively, these assignments agree well with those proposed previously on the basis of a CASPT2 computational study.[60] However, because the active space used in the CASPT2 calculations did not include a number of important frontier orbitals, the corresponding excited-state description is somewhat incomplete.

Electronic Structure of Co^{1+}Cbl. The good agreement between our spectroscopic and computational results for Co^{1+}Cbl strongly suggests that the closed-shell $3d^8$ singlet ground-state description for this species, as obtained from a PBE DFT calculation on our truncated Co^{1+}Cbl model, is correct. In particular, the close correspondence between the DFT-computed and experimentally determined frequencies of the corrin-based normal modes of vibration indicates that in Co^{1+}Cbl the corrin π system contains the same number of electrons as in Co^{2+} and Co^{3+}corrinoids, namely 14. Additionally, much poorer agreement would be achieved between our experimental and TDDFT-computed Abs spectra if the computation yielded an incorrect ground state wave function. Consequently, our experimentally validated electronic structure description for Co^{1+}Cbl developed in this work eliminates the possibility that this species possesses an open-shell antiferromagnetically coupled Co $3d^7$/corrin radical ground state, which was proposed previously on the basis of DFT computations using the B3LYP hybrid density functional.[56] The discrepancy between the current PBE results and the previous B3LYP results could be due to a number of factors, but the most likely source is the fundamentally different treatment of the exchange energy in the two methods. This example highlights the importance of an experimental validation of the results obtained using DFT methods, especially when applied to a simplified model of a large molecule such as the cobalamin cofactor.

The closed-shell $3d^8$ singlet ground-state electron configuration for Co^{1+}Cbl, as predicted by our PBE DFT computations, provides an intuitively appealing explanation for the "supernucleophilic" nature of this species.[10,11] Specifically, the large destabilization of the Co $3d_{z^2}$-based HOMO relative to the other filled MOs and its perpendicular orientation with respect to the corrin macrocycle renders nucleophilic attack both electronically and sterically facile. In enzymatic systems, it is conceivable that tuning of Co^{1+}Cbl's nucleophilicity, through perturbation of the energy of the $3d_{z^2}$-based HOMO, could protect the enzyme from deleterious side reactions, such as the attack of nonsubstrate molecules including enzymatic residues, or, alternatively, enhance the rate of nucleophilic attack on substrate (e.g., through H bonding to the Co^{1+} center, which would stabilize the HOMO, or by positioning an endogenous ligand in close proximity to the Co^{1+} center, which would destabilize the HOMO). Therefore, an important result from this work is that we have identified a clear spectroscopic marker for any enzymatic tuning of the energy of the $3d_{z^2}$-based HOMO, and thus the nucleophilicity, of Co^{1+}Cbl in the form of band 3 (Figure 5, Table 2), which is particularly prominent in the corresponding CD spectrum.[92] Because the donor orbital involved in the electronic transition responsible for band 3 possesses 94% Co $3d_{z^2}$ orbital character (Table 4), a blue-shift of this band will signify a stabilization of the $3d_{z^2}$-based HOMO and, thus, a decrease in the nucleophilic power of Co^{1+}Cbl. Conversely, a red-shift of band 3 will signify a destabilization of the HOMO and, thus, an increase in the nucleophilicity of Co^{1+}Cbl.

Implications for the Mechanism of Base-Off Co^{2+}Cbl → Co^{1+}Cbl Conversion. Having validated our PBE DFT calculations for Co^{1+}Cbl on the basis of our spectroscopic data, it is now reasonable to use the same computational approach for investigating mechanistic details for the reduction of base-off, 5-coordinate Co^{2+}Cbl to 4-coordinate Co^{1+}Cbl—a reaction catalyzed by a number of enzymatic systems, including MetH and ATR.[13−16,93] A particularly intriguing aspect of this reaction is that the in vivo reducing agents typically possess reduction midpoint potentials that are considerably more positive than that of the $Co^{2+/1+}$ couple of unbound base-off Co^{2+}Cbl ($E° = -500$ mV).[5]

Two fundamentally different mechanisms for the reduction of base-off, 5-coordinate Co^{2+}Cbl to 4-coordinate Co^{1+}Cbl can be invoked; namely, one where $Co^{2+} \rightarrow Co^{1+}$ reduction precedes the dissociation of the axially bound water molecule and the other where dissociation of the axially bound water molecule precedes $Co^{2+} \rightarrow Co^{1+}$ reduction (Figure 10). To assess the feasibility of the first mechanism, we have performed a single-

(92) Note that band 3 occurs in a region where proteins are optically transparent, thus ensuring that the nucleophilicity of enzyme-bound Co^{1+}Cbl can be probed at room temperature under physiologically relevant conditions.
(93) Jarrett, J. T.; Hoover, D. M.; Ludwig, M. L.; Matthews, R. G. *Biochemistry* **1998**, *37*, 12649−12658.

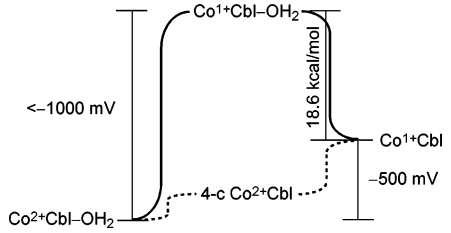

Figure 10. Semiquantitative reaction profile for the reduction of base-off, 5-coordinate Co^{2+}Cbl (Co^{2+}Cbl-OH_2) to 4-coordinate Co^{1+}Cbl for two distinct mechanistic pathways. Solid line: reduction of Co^{2+}Cbl to generate Co^{1+}Cbl-OH_2 precedes the dissociation of the axially bound H_2O molecule. Dashed line: dissociation of the axially bound H_2O molecule to form 4-coordinate Co^{2+}Cbl (4-c Co^{2+}Cbl) precedes the reduction to Co^{1+}Cbl. The overall reaction has an experimentally determined reduction potential of −500 mV vs SHE.[5]

point computation on a hypothetical 5-coordinate Co^{1+}Cbl species in which all atoms were kept at their DFT-optimized positions obtained for the base-off, 5-coordinate Co^{2+}Cbl model ($Co-OH_2$ bond of 2.35 Å). This species was found to be 18.6 kcal/mol higher in energy than separated 4-coordinate Co^{1+}-Cbl and H_2O (Figure 10), strongly suggesting that formation of a 5-coordinate Co^{1+}Cbl intermediate during the enzymatic conversion of Co^{2+}Cbl to Co^{1+}Cbl is energetically unfeasible. In contrast, by destabilizing the Co^{2+}Cbl reactant state via ligand dissociation prior to reduction, as invoked in the second mechanism, the overall reaction barrier remains unchanged, and the thermodynamically challenging $Co^{2+} \rightarrow Co^{1+}$ reduction is now separated into two biologically accessible steps. Collectively, these results suggest that the conversion of base-off, 5-coordinate Co^{2+}Cbl to 4-coordinate Co^{1+}Cbl is energetically accessible via formation of a 4-coordinate Co^{2+}Cbl intermediate, but not a 5-coordinate Co^{1+}Cbl intermediate. It is, thus, not surprising that effectively 4-coordinate Co^{2+}Cbl species have recently been observed for two members of the ATR family of enzymes, where this mode of substrate activation has been shown to correlate directly with a significant stabilization of the redox-active Co $3d_{z^2}$-based MO.[20,94]

Spectroscopic Trends within the Family of Corrinoids. The results from this work, along with those obtained in our recent spectroscopic and computational studies of Co^{3+} and Co^{2+}-corrinoids,[61,62] provide an excellent framework for exploring spectroscopic trends within this diverse family of cofactors. Here, we focus on two particularly striking trends, one regarding the vibrational features and the other concerning the Abs spectra of corrinoids.

SA Stretching Mode. On the basis of our DFT-assisted analysis of the rR spectra of Co^{1+}Cbl, the frequency of the corrin-based symmetric SA stretching mode (Figure 6, top) decreases considerably with decreasing positive charge on the Co center. This correlation between the frequency of the SA stretch, and thus the strength of the corrin π bonds oriented along the short axis of the corrin ring, and the positive charge on the Co center can be readily understood in terms of our PBE DFT computed MO diagram for Co^{1+}Cbl (Figure 9). Inspection of the isosurface plots for the low-lying empty orbitals reveals that the cor π*-based MOs possess substantial Co $3d_{xz}$ and $3d_{yz}$ orbital character (MOs cor π_8*−π_{10}*, Figure 9), signifying extensive mixing between the filled Co $3d_{xz}$ and $3d_{yz}$ orbitals and the empty cor π* frontier orbitals, The extent of this Co 3d → cor π* back-bonding is controlled by the energy separation between the interacting orbitals and, therefore, increases from Co^{3+}Cbls (where the filled Co 3d orbitals are too low in energy to engage in strong bonding interactions with the cor π* orbitals) to Co^{2+}Cbl and Co^{1+}Cbl.

Although not directly obvious from the isosurface plots of the cor π*-based MOs in Co^{1+}Cbl (Figure 9), this π-back-bonding apparently has a much greater effect on the frequency of the SA stretch than it does on the frequency of the LA stretch (vide supra). Importantly, regardless of Co oxidation state, the SA stretching mode of corrinoids can be readily identified in rR experiments by carrying out H → D exchange at the C_{10} position of the cofactor. Hence, rR spectroscopy potentially offers an excellent tool for probing changes in the positive charge on the Co center (e.g., via modulation of the donor strength of the axial ligand(s)) upon incorporation of the cofactor into enzyme active sites. To date, the only enzymatic system for which the SA stretching mode has been identified is the AdoCbl-dependent glutamate mutase (GM).[95] The SA stretching mode of AdoCbl was shown to upshift by a mere 1 cm^{-1} upon cofactor binding to the enzyme, despite the fact that this step involves a ligand switch in the lower axial position from the intramolecular DMB to a protein-derived His residue. Consequently, this axial ligand switch appears to have negligible effects on the electronic properties of the Co center, consistent with the conclusions drawn from a recent Abs and MCD spectroscopic study of GM.[96]

α-Band Transition. The most striking trend concerning the electronic spectra of corrinoids is the blue-shift of the lowest energy cor $\pi \rightarrow$ cor π* transition with decreasing formal oxidation state of the Co center from MeCbl (17 870 cm^{-1}) to Co^{2+}Cbl (21 050 cm^{-1}) and, finally, to Co^{1+}Cbl (25 700 cm^{-1}).[61,62] In each case, this transition primarily involves cor $\pi_7 \rightarrow$ cor π_8* one-electron excitation (see Figure 9 for Co^{1+}-Cbl), corresponding to the HOMO → LUMO transition of the metal-free corrin macrocycle. The energy of this transition, which is responsible for the so-called α/β-bands in the Abs spectra of Co^{3+}Cbls,[61] is determined by two basic factors. First, as noted previously,[61] the donor MO for this transition (corresponding to the cor π_7 orbital of Co^{1+}Cbl, Figure 9) becomes increasingly more destabilized with increasing σ-donor strength of the axial ligand(s). This relationship is particularly important for the 6-coordinate Co^{3+}Cbls, where the σ-donor strength of the upper axial ligand (e.g., the methyl group in MeCbl) directly controls the extent of the σ-antibonding interaction between the Co center and the lower axial DMB ligand; hence, the α/β-bands exhibit a progressive red-shift from, for example, H_2-OCbl—possessing a very weak σ-donor in the upper axial position—to MeCbl. Second, the relative energy of the acceptor MO for this transition (corresponding to the cor π_8* orbital of Co^{1+}Cbl, Figure 9) increases with a decreasing formal oxidation state of the Co center. This trend can be understood in terms of the π-back-bonding interactions that exist between the filled Co 3d and empty cor π* orbitals. Specifically, as the formal Co oxidation state decreases from +3 to +2 and +1, the extent of π-back-bonding from the filled Co $3d_{yz}$ orbital into the LUMO

(94) Stich, T. A.; Buan, N. R.; Escalante-Semerena, J. C.; Brunold, T. C. *J. Am. Chem. Soc.* **2005**, *127*, 8710−8719.
(95) Huhta, M. S.; Chen, H.-P.; Hemann, C.; Hille, C. R.; Marsh, E. N. G. *Biochem. J.* **2001**, *355*, 131−137.
(96) Brooks, A. J.; Fox, C. C.; Marsh, E. N. G.; Vlasie, M.; Banerjee, R.; Brunold, T. C. *Biochemistry* **2005**, *44*, 15167−15181.

of the corrin π system increases and, thus, the unoccupied cor π_8*-based MO becomes increasingly more destabilized relative to the filled cor π_7-based MO. Consequently, the α-band exhibits a steady blue-shift with decreasing positive charge on the Co center, and the energy of this feature may therefore be used as an experimental probe of the change in Co charge upon incorporation of the cofactor into an enzyme active site.

Although it has been noted previously that the specific combination of the Co ion and the corrin ring in MeCbl and AdoCbl likely allow for the formation of a delicately tuned source of a methyl cation and an Ado$^\bullet$ radical, respectively,[61] the spectroscopic trends discussed above provide additional clues as to why the B_{12} cofactors consist of a cobalt ion coordinated by a corrin macrocycle rather than a porphyrin ligand. Most importantly, as revealed by the dowsnhift of the SA strechting mode and the blue-shift of the lowest energy cor $\pi \rightarrow \pi^*$ transition with decreasing formal Co oxidation state, the corrin ring possesses empty π* orbitals that are sufficiently low in energy to allow for substantial π-back-bonding from the filled Co 3d orbitals. Consequently, the Co^{2+}/Co^{1+} redox couple falls within the physiologically accessible range, thus permitting methyl-transfer reactions and AdoCbl biosynthesis via formation of the Co^{1+}Cbl "supernucleophile" to occur. Alternatively, being a monoanionic ligand, the corrin macorcycle remains a sufficiently strong σ-donor to allow access to the Co^{3+} oxidation state. Specifically, as evidenced by the large variation in the peak positions of the α/β-bands in the Abs spectra of Co^{3+}-Cbls, the formally unoccupied Co $3d_{z^2}$ orbital contributes substantially to the cor π-based HOMO in these species, indicating that the extent of cor $\pi \rightarrow Co^{3+}$ 3d charge donation must be quite significant.

Acknowledgment. This work was supported by the NSF (CAREER grant MCB-0238530). We acknowledge Dr. Troy Stich for useful discussions and for collecting preliminary Abs, CD, and Raman data of Co^{1+}Cbl. The authors also thank Dr. Frank Neese (University of Bonn) for a free copy of his ORCA software package.

Supporting Information Available: Additional rR data of Co^{1+}Cbl, optimized geometries and thermochemical data for 4- and 5-coordinate computational models of Co^{1+}Cbl, as well as the relevant output from additional geometry optimizations, DFT frequency calculations, and TDDFT excited-state computations not presented in the text. This material is available free of charge via the Internet at http://pubs.acs.org.

JA061433Q